Journal of Inorganic and Organometallic Polymers and Materials
https://doi.org/10.1007/s10904-021-01966-7

Synthesis, Structure, and Properties of a Dinuclear Cu(II) Coordination Polymer Based on Quinoxaline and 3,3-Thiodipropionic Acid Ligands

Adedibu C. Tella[1,3] · Samson O. Owalude[1] · Vincent O. Adimula[1,2,5] · Adetola C. Oladipo[1] · Victoria T. Olayemi[1] · Bushra Ismail[2] · Amara Mumtaz[2] · Attiq Ur Rehman[2] · Asad M. Khan[2] · Hadley S. Clayton[3] · Nawaz M. Tahir[4]

Received: 7 December 2020 / Accepted: 5 March 2021
© The Author(s), under exclusive licence to Springer Science+Business Media, LLC, part of Springer Nature 2021

Abstract
The coordination polymer $[Cu_2(TDPH)_4(QNX)]$.DMF, (QNX = Quinoxaline; TDPH = 3,3-thiodipropionic acid), has been prepared by reaction of copper acetate, TDPH, and quinoxaline. The compound was characterized by elemental analysis, FTIR spectroscopy, and single-crystal X-ray diffraction. The crystal is monoclinic with a P21/n space group and dimensions of a = 12.889(3) Å, b = 14.983(4) Å, c = 14.091(3) Å, α = 90°, β = 90.200(11)°, γ = 90°, V = 2721.18 (2) $Å^3$, Z = 4. The ligands are hexagonally coordinated to the Cu(II) centre in the form of Cu_2O_4N with one nitrogen atom from the quinoxaline ligand, and four oxygen atoms from four TDPH molecules in a monodentate fashion. The Cu–Cu bond length was 2.642(1) and 2.629(1) Å for the Cu1–Cu1 and Cu2–Cu2 bonds. The QNX ligand bridged the two copper atoms. The catalytic reduction of 4-nitrophenol to 4-aminophenol using $NaBH_4$ in the presence of $[Cu_2(TDPH)_4(QNX)]$.DMF, as catalyst was completed within 11 min. The 4-aminophenol product was confirmed using ^1H NMR spectroscopy.

Keywords Coordination polymer · Quinoxaline · 3,3-Thiodipropionic acid · Nitrophenol · Aminophenol

1 Introduction

Coordination polymers have attracted a lot of attention over the decades because of their interesting properties, synthetic routes and rich chemistry. Synthesis through the solvent-free and solvent-based techniques have been reported [1, 2]. Research into the preparation of coordination polymers/networks have led to the discovery of materials such as metal–organic frameworks which have advanced functionalities [2–6].

Porous coordination polymers have evolved as a class of versatile and attractive functional porous materials. They are made up of organic molecules connected by metal ions in a uniform porous network which incorporates sufficient stability and chemical resistance to most solvents [6, 7]. Porous coordination polymers have over the years emerged as an important group of porous hybrid materials with diverse potential applications including catalysis [8], gas storage [9], luminescence and molecular sensing [10, 11], including drug loading and delivery [12]. Coordination polymers are usually prepared under conditions which allow for tunable structure and incorporation of building blocks with desired functions thereby making them suitable for specific purposes [8]. These class of compounds are also characterized by large surface area and well-defined reaction environments which increases their potential applications in the area of heterogeneous catalysis [13]. Chiral ligands such as 1,1′-bi-2-naphthol, porphyrins, and their derivatives have been used as building blocks in the preparation of coordination polymers for specific usage as asymmetric catalysts [11–13]. The incorporation of molecular structures with catalytic attributes enables

✉ Adedibu C. Tella
ac_tella@yahoo.co.uk

✉ Vincent O. Adimula
vincentadimula@gmail.com

1 Department of Chemistry, University of Ilorin, P.M.B.1515, Ilorin, Kwara State, Nigeria

2 Department of Chemistry, COMSATS University, Abbottabad Campus, Islamabad 22060, Pakistan

3 Department of Chemistry, University of South Africa, Pretoria, South Africa

4 Department of Physics, University of Sargodha, Sargodha, Punjab, Pakistan

5 Department of Industrial Chemistry, University of Ilorin, P.M.B.1515, Ilorin, Kwara State, Nigeria

Published online: 24 March 2021

Content courtesy of Springer Nature, terms of use apply. Rights reserved.

the possibility of the spatial control to obtain coordination polymers with synergistic catalytic effect [7, 14, 15]. Their stability and chemical resistance in most solvents have made them materials of great interest in chemical separation and heterogeneous catalysis [15–19].

Coordination polymers provide an interesting platform for the preparation of luminescent solid-state materials due to their well-defined structural morphology [14, 17]. Coordination polymers with luminescent properties have been isolated for some time with the first report appearing in 2002 [13, 16]. Thereafter, various researches have been focused on the exploitation of their light emission properties to generate functional materials [18–20]. The possibility of incorporating permanent porosity into their structures is responsible for the luminescence features of coordination polymers. The immobilization of guest molecules, in the pores, close to luminescent centres may lead to a shift in wavelength, which affects their emission properties [18]. Coordination polymers developed with luminescent properties have been applied in sensing and detection of molecules. The observed luminescence could originate from the metal ion or the organic ligand with a conjugated system [19]. Lanthanide coordination polymers have been reported lately with fascinating photoluminescence properties. Polymetallic lanthanide coordination polymers reported by White et al. [19], were shown to simultaneously emit numerous near-infrared signals due to the different lanthanide ions present. Strong luminescent emission peaks observed in a tetranuclear Cu(II)-based coordination polymer were attributed to the presence of conjugated ligand systems in the structure [20]. Conjugation upon coordination with metal ions enhance greatly the luminescence properties of coordination polymers [19, 22]. Those with structures constructed from carboxylate ligands have been reported to exhibit conjugation upon coordination with metal ions [21]. Several coordination polymers based on carboxylate ligands have therefore been reported with exciting catalytic and luminescence properties.

In this study, we utilized a combination of carboxylate and nitrogen donor linkers to prepare a dinuclear Cu(II) coordination polymer. To the best of our knowledge, there is no report of such dinuclear Cu(II) coordination polymer having a combination of quinoxaline and 3,3-thiodipropionic acid ligand system. The conjugated system of the quinoxaline ligand was exploited to incorporate additional luminescence property to the material along with the Cu(II) ion while the carboxylate linker was chosen to achieve a porous network structure. Thus, we herein report the synthesis, crystal structure, luminescence, and catalytic property of a coordination polymer assembled using Cu(II) ion, quinoxaline, and 3,3-thiodipropionic acid, and formulated as $[Cu_2(TDPH)_4(QNX)].DMF$.

2 Experimental Section

2.1 Materials and Methods

Quinoxaline and 3,3-thiodipropionic acid were commercially sourced from Sigma Aldrich and were used as received. The hydrated Cu(II) salt ($Cu(CH_3COO)_2{\cdot}H_2O$), dimethylformamide (DMF), and ethanol were purchased from British Drug House (BDH) Poole, England. The melting point of $[Cu_2(TDPH)_4(QNX)].DMF$ was determined using a Gallen-Kamp melting point apparatus. This is to determine the stability of the compound under increased temperature. The compound $[Cu_2(TDPH)_4(QNX)].DMF$ was observed to have a melting point > 400 °C. Elemental analysis to determine the percentage of C, H, and N was carried out with a Carlo Erba Model EA1108 elemental analyzer. Thermogravimetric analysis was carried out on a TGA Q500 V6.7 Build 203 thermogravimetric analyser in the presence of nitrogen. FTIR analysis of the compound was carried out using KBr pellets on FTIR 8400s Shimadzu spectrophotometer. Brunauer–Emmett–Teller surface area measurements of $[Cu_2(TDPH)_4(QNX)].DMF$ was carried out by N_2 adsorption experiments on a NOVA 4200e BET instrument. The fluorescence spectra of the compound and the ligands were recorded on a Perkin Elmer LS45 Fluorescence spectrophotometer using DMSO as a solvent. The ^1H NMR spectra were obtained using a Bruker Avance 400 MHz NMR instrument with D_2O as a solvent. Powder X-ray diffraction (PXRD) was carried out on a Siemens D5000 diffractometer.

2.2 Synthesis of the Dinuclear $[Cu_2(TDPH)_4(QNX)].DMF$

A mixture of 3,3-thiodipropionic acid (0.178 g, 1 mmol) in 10 ml DMF and quinoxaline (0.130 g, 1 mmol) in 10 ml ethanol was added to a solution of $Cu(CH_3COO)_2{\cdot}H_2O$ in 10 ml distilled water. The resultant solution was heated to reflux at 120 °C for 2 h under constant stirring at 1000 rpm. The solution was allowed to cool to room temperature, and after 90 days, blue crystals suitable for x-ray crystallographic analysis were obtained.

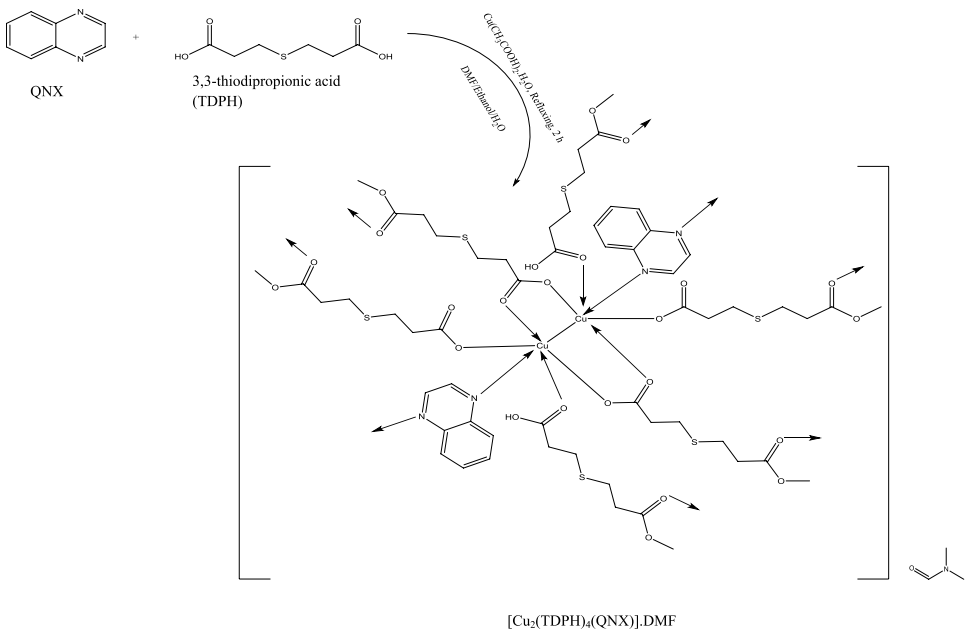
Yield: 78%, M. Wt.: 684.592 g/mol^{-1}, melting pt.: > 400 °C, elemental analysis (%): calc. (found) C, 78.2 (78.9); H, 8.47 (9.01); N, 11.8 (12.0), IR (KBr pellets (cm^{-1}): 158, 1748, 1605 (Scheme 1).

2.3 Crystallographic Data Collection and Structural Analysis

The X-ray data were collected on graphite-monochromated MoKα radiation (λ = 0.71073 Å) Bruker Kappa Apex II

Content courtesy of Springer Nature, terms of use apply. Rights reserved.

Scheme 1 Reaction scheme for the synthesis of $[Cu_2(TDPH)_4(QNX)].DMF$



CCD diffractometer. The crystals were mounted using cryoloops with Paratone-N oil. By intrinsic phasing using SheLXS structure solution program, $[Cu_2(TDPH)_4(QNX)].DMF$ structure was solved using Olex2 and the ShelXL was used as the refinement package by Least Squares minimization. The crystal parameters, collection data and the refinements details are presented in Table 1.

2.4 Reduction of 4-Nitrophenol to 4-Aminophenol Catalyzed by $[Cu_2(TDPH)_4(QNX)].DMF$

The catalytic activity of coordination polymer $[Cu_2(TDPH)_4(QNX)].DMF$ in the reduction of 4-nitrophenol (4-NP) by $NaBH_4$ was investigated using a modified literature procedure [23, 24]. *p*-nitrophenol (0.001 mol/L) and sodium borohydride (0.1 mol/L) were prepared and mixed. A 15 ml aliquot of this was withdrawn and 4 mg of $[Cu_2(TDPH)_4(QNX)].DMF$ was added in a 25 ml beaker with stirring at 800 rpm. The rate of reduction process was followed with a UV–Vis spectrophotometer in the wavelength range of 250–600 nm.

3 Results and Discussions

The one-pot reaction of quinoxaline, 3,3-thiodipropionic acid and copper(II) acetate in a mixture of ethanol and water yielded $[Cu_2(TDPH)_4(QNX)].DMF$. Elemental analysis of $[Cu_2(TDPH)_4(QNX)].DMF$ conform with a mole ratio of 4:1:2 for 3,3-thiodipropionic acid, quinoxaline, and Cu(II) ion respectively, with one DMF molecule outside the coordination sphere.

Table 1 Crystal data and structure refinement for compound $[Cu_2(TDPH)_4(QNX)].DMF$

Compound reference	$[Cu_2(TDPH)_4(QNX)].DMF$
Empirical formula	$C_{23}H_{29}Cu_2N_3O_9S_2$
Formula weight	682.725
Temperature/K	296.15
Crystal system	Monoclinic
Space group	P $2_1/n$
aÅ	12.889(3)
bÅ	14.983(4)
cÅ	14.091(3)
α/°	90
β/°	90.200(11)
γ/°	90
Volume/Å^3	2721.18
Z	4
D_{cald} (g cm^{-3})	1.666
μ (Mo Ka) (mm^{-1})	1.772
F(000)	1404.5
h, k, l range	$3.968° \leq 2\theta \leq 56°$
Structure determination	SHELXS-97
Refinement method	Full-matrix least-squares on F^2
Reflections collected	6494
Independent reflections	6494 [Rsigma = 0.0631]
Parameters/restraints	355/0
Goodness of fit on F^2	1.089
Final *R* indexes [$I > 2\sigma$ (*I*)]	R1 = 0.0499, wR2 = 0.1279
Final R indexes (all data)	R1 = 0.0780, wR2 = 0.1419
Largest diff. peak hole/e Å^{-3}	0.92/−1.01

Content courtesy of Springer Nature, terms of use apply. Rights reserved.

Measurements of the porosity and surface area of compound $[Cu_2(TDPH)_4(QNX)].DMF$ was carried out by N_2 adsorption experiments. The Brunauer–Emmet–Teller (BET) analysis and Langmuir equations showed the specific surface area to be 213.765 $m^2\ g^{-1}$ (709.005 $m^2\ g^{-1}$ Langmuir) which is comparable with BET values of some previously reported similar compounds [2, 23–28]. The pore volumes and sizes were observed to be 0.069 $cm^3\ g^{-1}$ and 2.647 nm respectively. The BET nitrogen isotherm of $[Cu_2(TDPH)_4(QNX)].DMF$ is presented in Fig. S1 in the supplementary information.

3.1 Description of the Crystal Structure of $[Cu_2(TDPH)_4(QNX)].DMF$

ORTEP diagram of $[Cu_2(TDPH)_4(QNX)].DMF$ is presented in Fig. 1 and the polymeric view showing the paddle-wheel structure is given in Fig. 2. The interatomic bond lengths and angles around the Cu(II) ion are given in Table 1. Two Cu(II) ions are present in the structure each having an octahedral geometry with the carboxylate group of one of the 3,3-thiodipropionic acid coordinating in a bidentate mode. The two Cu(II) ions bonded to each other with a bond length of 2.642(1) and 2.629(1) Å for the Cu1–Cu1 and Cu2–Cu2 bonds indicating a weak interaction between the Cu atoms. One of the TDPH ligands was observed to bridge the two copper ions via the O1A and O2A of the C9A of the carboxylate group with bond lengths of 1.965 and 1.945 Å favourably comparing with the bond length range of 1.911–1.998 Å observed for Cu–O bonds in similar compounds [8, 22, 24–28]. The quinoxaline molecules coordinated to the Cu(II) ions through the N1C and N2C atoms in a monodentate manner (Cu1–N1C = 2.287 Å, Cu2–N2C = 2.263 Å) with bond lengths within the range of 1.98–2.328 Å reported in literature for N–Cu(II) interactions in similar compounds having the Cu–N bonds [27, 28]. Bond angles of the ligands around Cu(II) ions were observed to be 167.5° for the O1A Cu1 O2A, and 98.8° for the O1A Cu1 N1C. Intermolecular hydrogen bonds of the O–H–O type were observed in the structure from the O1A and the O–H–N-type from the O7BA. Hydroxyl O2A and O7B act as proton donors while the coordinated O1A and O2A of the carboxylate groups act as proton acceptors [28]. The polymeric view of $[Cu_2(TDPH)_4(QNX)].DMF$ in Fig. 2 showed the formation of a paddle-wheel structure by the Cu atoms with the quinoxaline and 3,3-thiodipropionic acid ligands.

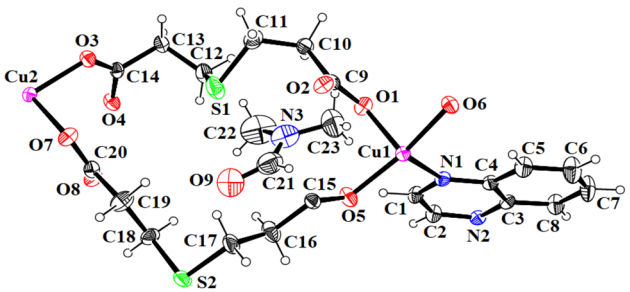


Fig. 1 ORTEP diagram of $[Cu_2(TDPH)_4(QNX)].DMF$

3.2 PXRD Results

The PXRD pattern (experimental and simulated) of $[Cu_2(TDPH)_4(QNX)].DMF$ presented in Fig. 3 indicates the purity of the $[Cu_2(TDPH)_4(QNX)].DMF$ compound prepared. Orientation preferences is proposed as a reason for the differences observed in the peak intensities, where the simulated pattern represents diffraction from the $[Cu_2(TDPH)_4(QNX)].DMF$ crystal planes while the experimental pattern may not include all crystal planes.

3.3 FTIR Analysis

The antisymmetric stretching vibrational mode of COO^- (ν_{asym} (COO^-)) is observed at 1567 cm^{-1} in $[Cu_2(TDPH)_4(QNX)].DMF$, a value lower than 1572 cm^{-1} in the free TDPH ligand suggesting coordination through the COO^- group of the TDPH [28–30]. In the uncoordinated TDPH, the symmetric COO^- (ν_{sym} (COO^-)) appear at 1315 cm^{-1} but shifted to a value of 1409 cm^{-1}, attributed

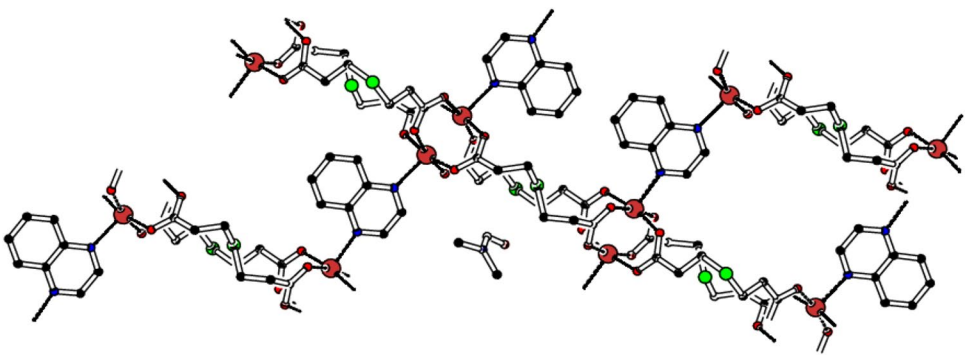


Fig. 2 Polymeric view of $[Cu_2(TDPH)_4(QNX)].DMF$ showing the Cu-atoms in a paddle-wheel coordination

Content courtesy of Springer Nature, terms of use apply. Rights reserved.

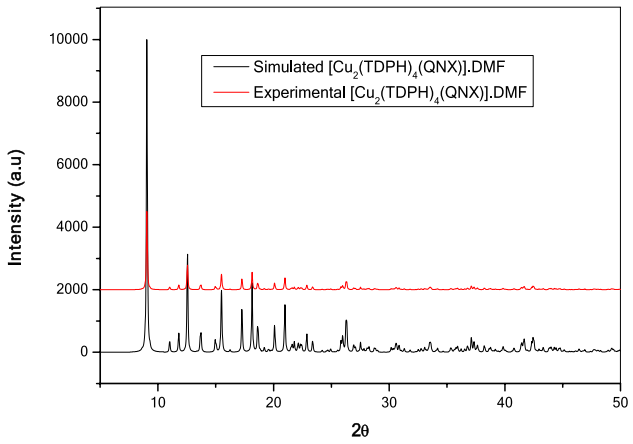


Fig. 3 PXRD pattern of the prepared $[Cu_2(TDPH)_4(QNX)].DMF$

to coordination through this group. The difference between the antisymmetric and symmetric stretching vibrations of the COO^- group $\Delta(\nu_{asym}\ (COO^-) - \nu_{sym}\ (COO^-))$ is 158 cm^{-1} suggesting a bridging bidentate coordination mode for the COO^- in $[Cu_2(TDPH)_4(QNX)].DMF$ [31]. This is in agreement with the results obtained from the X-ray crystallographic analysis of the compound. The ν(C=O) absorption band observed at 1752 cm^{-1} in the TDPH ligand was shifted to a lower frequency at 1748 cm^{-1} suggesting that the coordination of the carboxylate group to the Cu(II) ion in **1** is via the carbonyl group [29]. The ν(C–O) absorption band observed at 1105 cm^{-1} in the free ligand was shifted to 1094 cm^{-1} in $[Cu_2(TDPH)_4(QNX)].DMF$. Absorption band attributable to the ν(C=N) observed at 1612 cm^{-1} in the free quinoxaline ligand was shifted to lower frequency at 1605 cm^{-1} in $[Cu_2(TDPH)_4(QNX)].DMF$, suggesting that the coordination of the quinoxaline to the Cu(II) ion is via one of the nitrogen atoms in the pyrazine ring of the ligand [28]. The spectra confirm the coordination of the quinoxaline ligand to the Cu(II) ion via one of the nitrogen atoms of the pyrazine ring and through the carboxylate group of the TDPH ligand. FTIR spectra of $[Cu_2(TDPH)_4(QNX)].DMF$ is presented in Fig. 4.

3.4 Thermal Analysis of $[Cu_2(TDPH)_4(QNX)].DMF$

Thermal analysis of compound $[Cu_2(TDPH)_4(QNX)].DMF$ presented in Fig. 5 shows that the first mass loss occurred between the temperature of 145–160 °C which corresponds to the loss of a DMF molecule present outside the coordination sphere. Thereafter, a major loss in mass was observed at a temperature of about 358 °C up to 390 °C attributable to the decomposition of one molecule of TDPH (calc./found: 26.0/26.4%). The next decomposition stage was observed between 390 and 420 °C which resulted

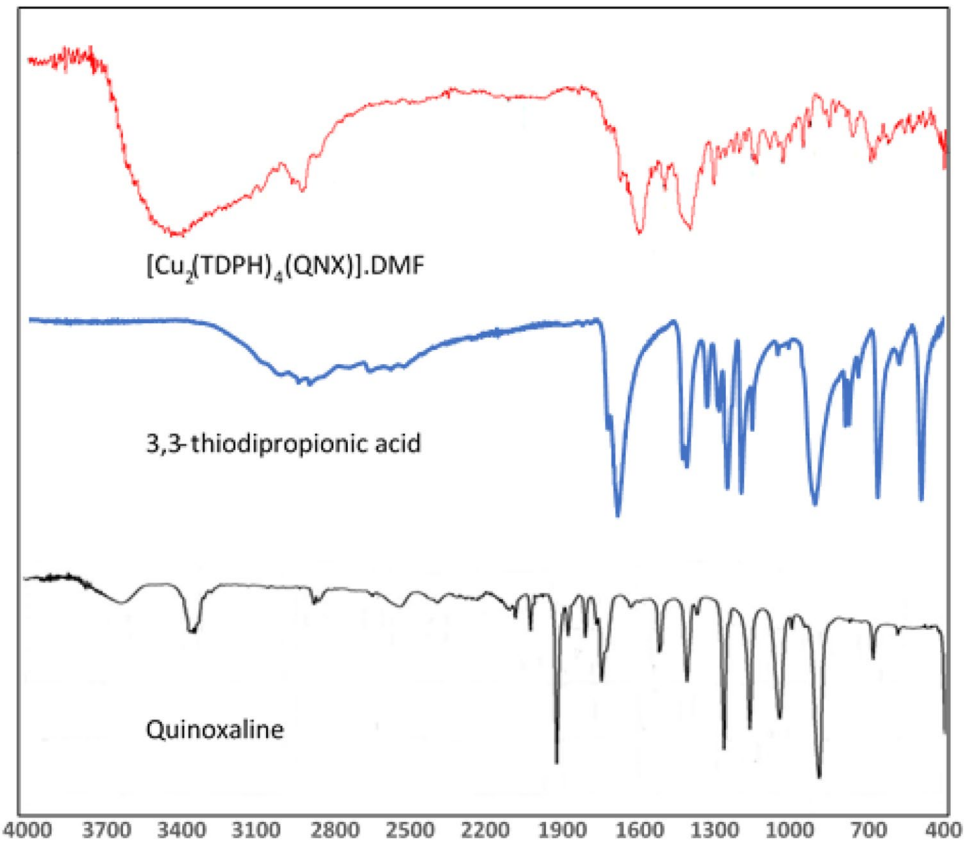


Fig. 4 FTIR spectra of $[Cu_2(TDPH)_4(QNX)].DMF$ and the free ligands

Content courtesy of Springer Nature, terms of use apply. Rights reserved.

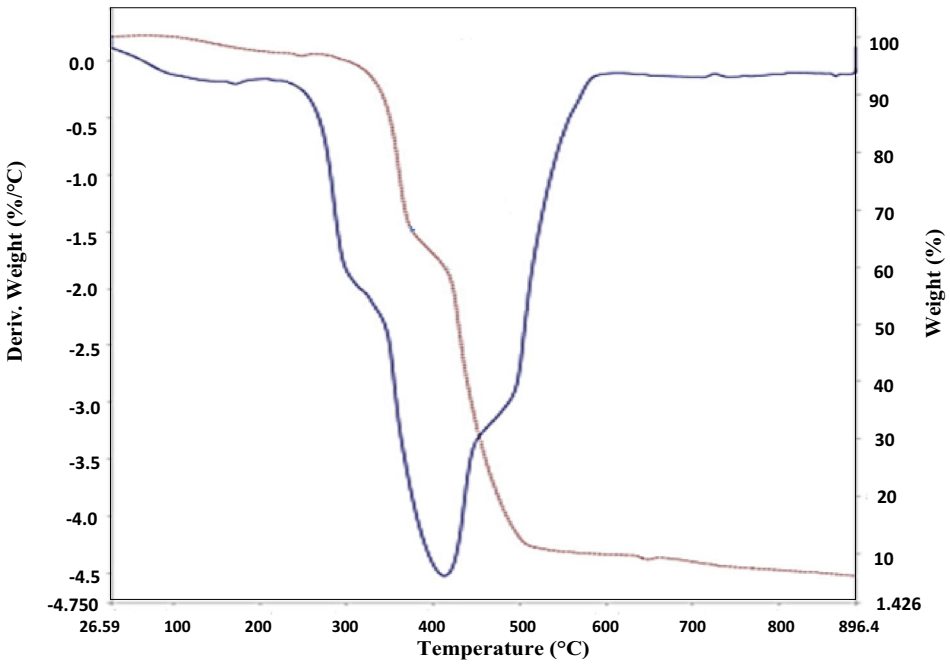


Fig. 5 TGA curve of compound $[Cu_2(TDPH)_4(QNX)].DMF$

in about 10% weight loss suggesting the loss of a molecule of DMF (calc./found: 10.67/10.19%) believed to have been trapped within the pores of $[Cu_2(TDPH)_4(QNX)].DMF$ [18]. Decomposition of the remaining organic backbone structure was observed between 420 and 510 °C, thereafter, the curve flattens [2, 25].

3.5 Photoluminescence Properties

Coordination polymers having the hydroxide motifs have been reported to exhibit photoluminescence properties [29, 33]. The photoluminescence spectra showing the fluorescence emission property of compound $[Cu_2(TDPH)_4(QNX)].DMF$ is presented in Fig. 6. It was observed that the excitation wavelength of 388 nm resulted in emission peaks observed at 401 nm and 547 nm, while the free ligands (quinoxaline and TDPH) exhibit photoluminescence emissions at 545 and 409 nm respectively [29]. The emission bands of 401 and 547 nm observed for compound $[Cu_2(TDPH)_4(QNX)].DMF$ may be derived from the different coordination environment of quinoxaline and TDPH and also ligand to metal charge transfer (LMCT) [29, 34]. The free ligands displayed luminescence characters at 409 and 545 nm respectively. Fluorescent intensity of quinoxaline ($\lambda_{emi} = 545$ nm) diminished upon coordination to the Cu(II) ion, this may be due to ligand centred electronic transition and may be a useful indicator for the use of $[Cu_2(TDPH)_4(QNX)].DMF$ as sensors in applications in which Cu(II) ions are being evaluated [33, 35].

3.6 SEM Results

The morphology of $[Cu_2(TDPH)_4(QNX)].DMF$ observed by scanning electron microscope (SEM) depicts the compounds as uniform crystalline block-like aggregates of regular shaped rectangles Fig. 7a. The particle size distribution of $[Cu_2(TDPH)_4(QNX)].DMF$ illustrated in Fig. 7b shows a somewhat uniform size distribution with a minimum particle size of 149 µm while the maximum was observed to be 159 µm. The uniform crystallinity and homogeneous nature of the material as seen in the SEM images positively influences the catalytic performance of the material.

3.7 Catalytic Activity Study

The UV–Vis spectra of the 4-NP at 317 nm was red-shifted to 400 nm (Fig. 8) upon introduction of $NaBH_4$ into the reaction medium, the colour of the solution changed to bright yellow from light yellow attributable to the presence of 4-nitrophenolate ion [34, 35]. The reduction process started with the introduction of $[Cu_2(TDPH)_4(QNX)].DMF$ into the reaction mixture and the progress of the reaction was monitored using UV–Vis spectrophotometer. Absorption band was observed at 300 nm upon addition of the catalyst, this is due to the conversion of 4-NP to 4-AP, which continued to increase in intensity while the band at 400 nm decreased in intensity with increase in reaction time [32–34]. The UV–Vis spectra of the reaction in which $NaBH_4$ is absent and present is presented in Fig. 8a and b, while Fig. 9 shows the UV–Vis spectra of the reaction upon addition of $[Cu_2(TDPH)_4(QNX)].DMF$ into the reaction medium.

Content courtesy of Springer Nature, terms of use apply. Rights reserved.

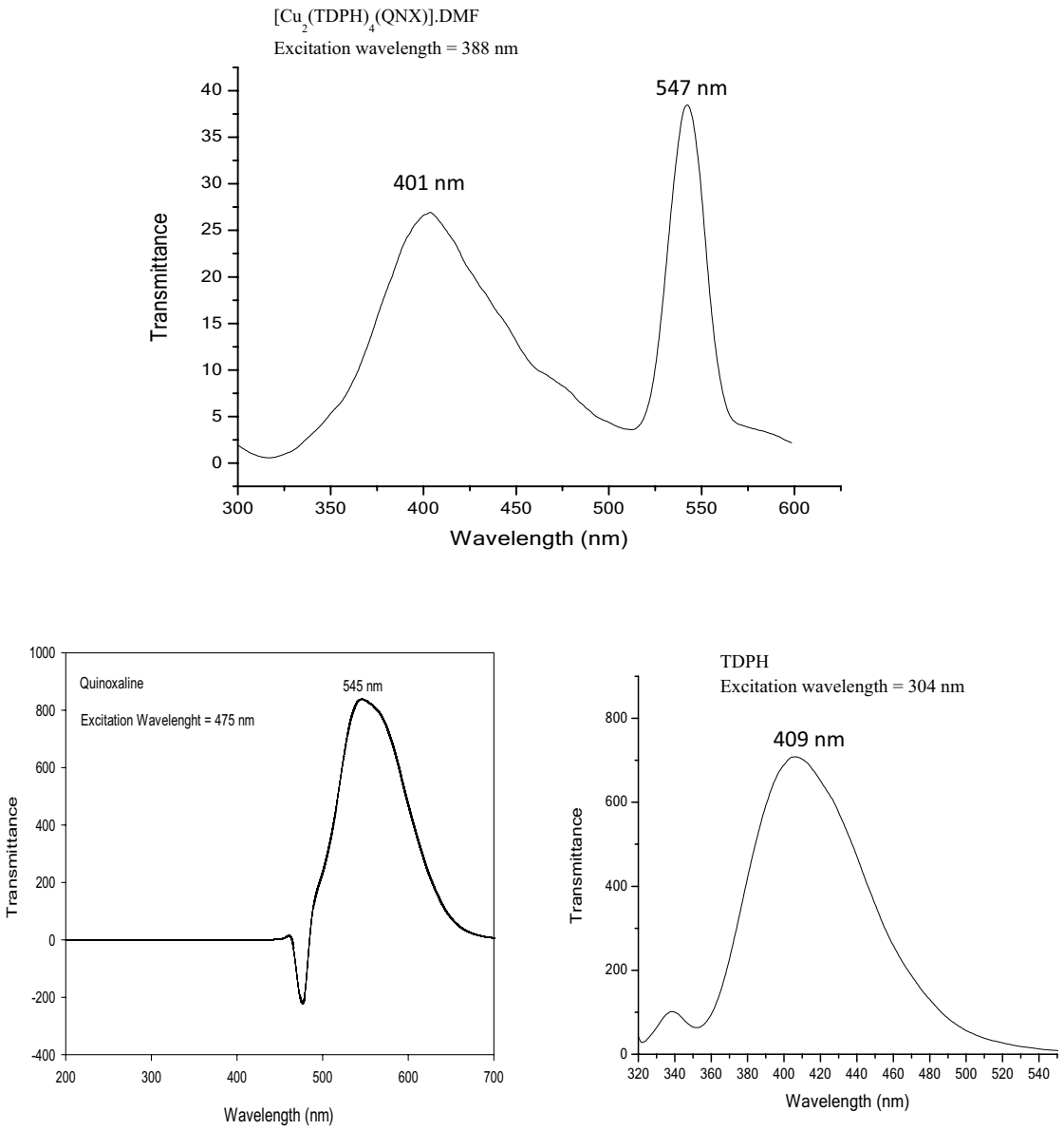


Fig. 6 Photoluminescence spectra of $[Cu_2(TDPH)_4(QNX)].DMF$, TDPH, and quinoxaline

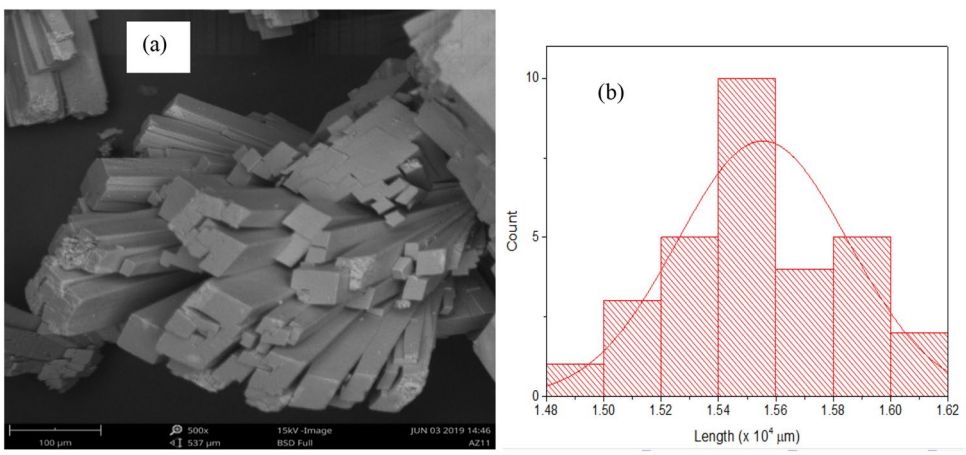


Fig. 7 **a** SEM images of the $[Cu_2(TDPH)_4(QNX)].DMF$ **1** crystal; **b** particle size distribution

Content courtesy of Springer Nature, terms of use apply. Rights reserved.

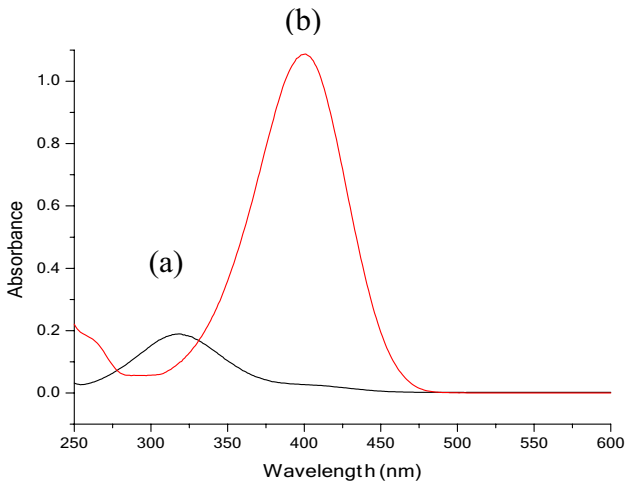


Fig. 8 Absorption spectra of 4-nitrophenol in (a) the absence of $NaBH_4$ (b) the presence of $NaBH_4$

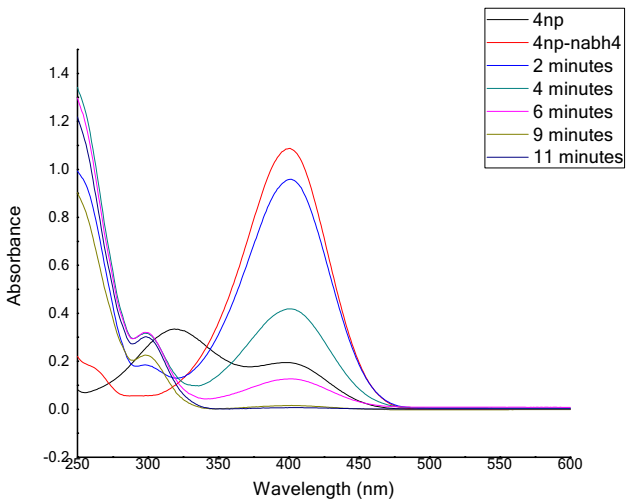


Fig. 9 UV–Vis spectra showing the reduction of 4-NP by $NaBH_4$ using the dinuclear $[Cu_2(TDPH)_4(QNX)].DMF$ coordination polymers as catalysts

The characteristic peak of 4-nitrophenol which was red-shifted to 400 nm disappeared completely after a reaction time of 11 min (Fig. 9) in the presence of $[Cu_2(TDPH)_4(QNX)].DMF$ as a catalyst. The colour of the reaction mixture faded from bright yellow to colourless at the end of the reaction.

3.8 Reduction Kinetics

The reduction kinetics for the reaction is represented by Eq. (1) [34, 36]:

$$r = \frac{dc}{dt} = \ln\frac{C_t}{C_o} = -k_{app}t \quad (1)$$

r = reactant reduction rate; t = reaction time; k_{app} = kinetic rate constant; c_t = concentration of 4-NP at time t; and c_o = initial concentration of 4-NP. Equation (1) above can also be written as [36]:

$$r = \frac{dc}{dt} = ln\frac{A_t}{A_o} = -k_{app}t \quad (2)$$

A_t and A_o represents absorbance at time t and 0 respectively. A plot of $\ln\frac{A_t}{A_o}$ against t, should give a straight-line graph with a slope $= -k_{app}$. Figure 10 presents the pseudo-first-order kinetic plots for the reduction of 4-nitrophenol using $NaBH_4$, in the presence of $[Cu_2(TDPH)_4(QNX)].DMF$ as catalysts.

The value of the rate constant (k) for the reduction process was calculated from the slope of the plot of $\ln(A_t/A_o)$ as 8.4×10^{-3} s^{-1}. Reports have indicated that reduction of 4-nitrophenol by $NaBH_4$ occurs by a transfer of an electron from the BH_4^- ion, facilitated by the catalyst, to the 4-nitrophenol, overcoming the kinetic barrier of the reaction, in the process, which would normally not have commenced in the absence of a catalyst [34–38]. This is supported by the control experiment which was carried out in the absence of $[Cu_2(TDPH)_4(QNX)].DMF$. No observable change was observed in the reaction mixture of 4-nitrophenol and $NaBH_4$ in the absence of $[Cu_2(TDPH)_4(QNX)].DMF$ as catalysts.

3.9 Thermodynamic Studies

The reduction reactions were carried out at four different temperatures of 30, 40, 50, and 60 °C. The results showed a decrease in the rate constant as temperature increases. An increase in rate constant was, however, observed at 60 °C. This is attributed to the increase in disorderliness at that

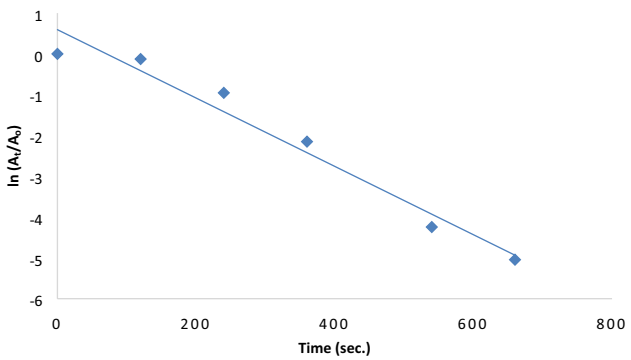


Fig. 10 Plot of ln (At/Ao) versus reaction time for the reduction of 4-NP using $[Cu_2(TDPH)_4(QNX)].DMF$ as catalyst

Content courtesy of Springer Nature, terms of use apply. Rights reserved.

temperature in agreement with the positive value of entropy obtained at this temperature [23]. Figure 11 represents a plot of ln (A_t/A_o) against time (s) at different temperatures while the corresponding rate constants are presented in Table 2.

3.10 Effect of Initial 4-NP Concentration

The dependence of the reaction rate on different concentrations of 4-nitrophenol was investigated and the rate constants were calculated at different concentrations of 4-NP. The results are presented in Fig. 12 and the parameters obtained from the plots in Table 3. The data in Table 3 indicates that the rate of the reduction process decreases as the concentration increases. This is due to the higher adsorption affinity for 4-NP by the catalyst compared to the BH_4^- ions giving rise to fewer adsorption sites for the BH_4^- [34, 35].

3.11 Catalytic Activity, Conversion Efficiency, and Turnover Frequency

The activity of the catalyst was estimated by taking the ratio of the rate constants to the weight of the catalyst used [38]. Conversion efficiency for the process was obtained using Eq. 3 while the turn over frequency (TOF) was calculated using Eq. 4 [38–42]

$$\%Reduction = 100 - \left(A_t \times 100/A_o\right) \tag{3}$$

$$TOF = \frac{m_i X x}{100\, wt} \tag{4}$$

where A_t = absorbance at time t, A_o = initial absorbance, m_i = initial no of moles of 4-NP, X = percentage conversion, x = molecular weight of 4-NP, w = mass of catalyst (g) and t = reaction time (h).

Table 2 Interatomic lengths and bond angles of $[Cu_2(TDPH)_4(QNX)].DMF$

Bond length (Å)		Bond angles (°)	
Cu1 O1A	1.965	O1A Cu1 O2A	167.5
Cu1 O2A	1.945	O1A Cu1 O8B	90.0
Cu1 O7B	1.963	O1A Cu1 N1C	98.8
Cu1 N1C	2.287	O1A Cu1 O7B	87.8
Cu1 O8B	1.980	O2B Cu1 O7B	90.6
Cu1 Cu1	2.642	O8B Cu1 N1C	100.3
		O2B Cu1 O8B	89.0
		O7B Cu1 N1C	92.0
		O7B Cu1 O8B	167.7
		N1C Cu1 O2B	93.7

The catalytic activity was estimated as 2.1 g^{-1} s^{-1} while the conversion efficiency was 99.4%, these values are comparable with the results obtained for other catalysts employed for the same reaction [41, 42]. The observed turnover frequency for the catalyst is 188.6 molecules g^{-1} s^{-1}.

3.12 Reusability Experiment

Reusability of $[Cu_2(TDPH)_4(QNX)].DMF$ as a catalyst for the reduction process was investigated by regenerating the spent catalyst. After each catalytic experiment, the catalyst was recovered from the solution by filtration, washed several times with distilled water, dried in the oven at 80 °C for 24 h and then reused. The results in Fig. 13 indicate that a substantial amount of $[Cu_2(TDPH)_4(QNX)].DMF$ can be recovered from the spent catalyst, an indication that it is reusable. The recovered catalyst is reusable over at least three cycles except that an increase in time required for the reduction reaction to complete was observed after each catalytic cycle.

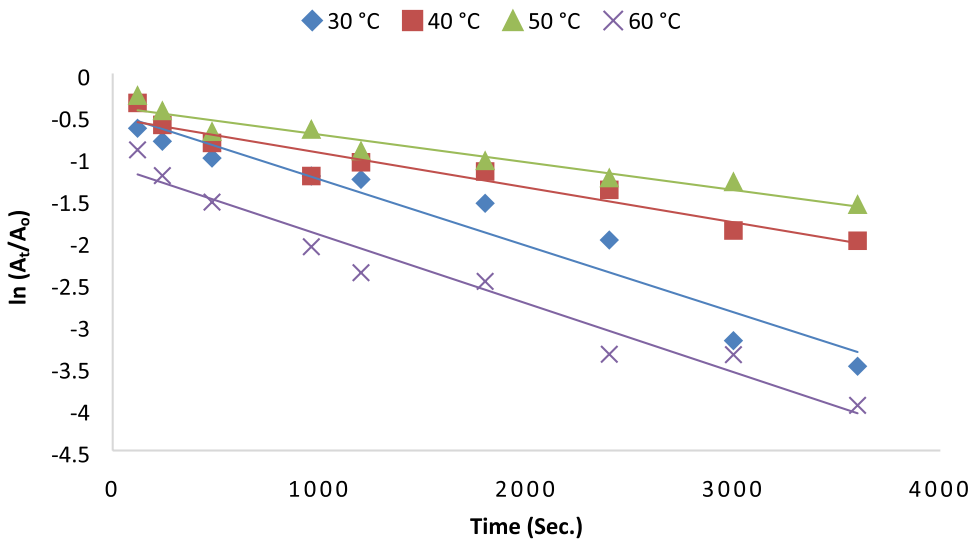


Fig. 11 Plots of ln (At/Ao) against time for the reduction of 4-NP at different temperatures

Content courtesy of Springer Nature, terms of use apply. Rights reserved.

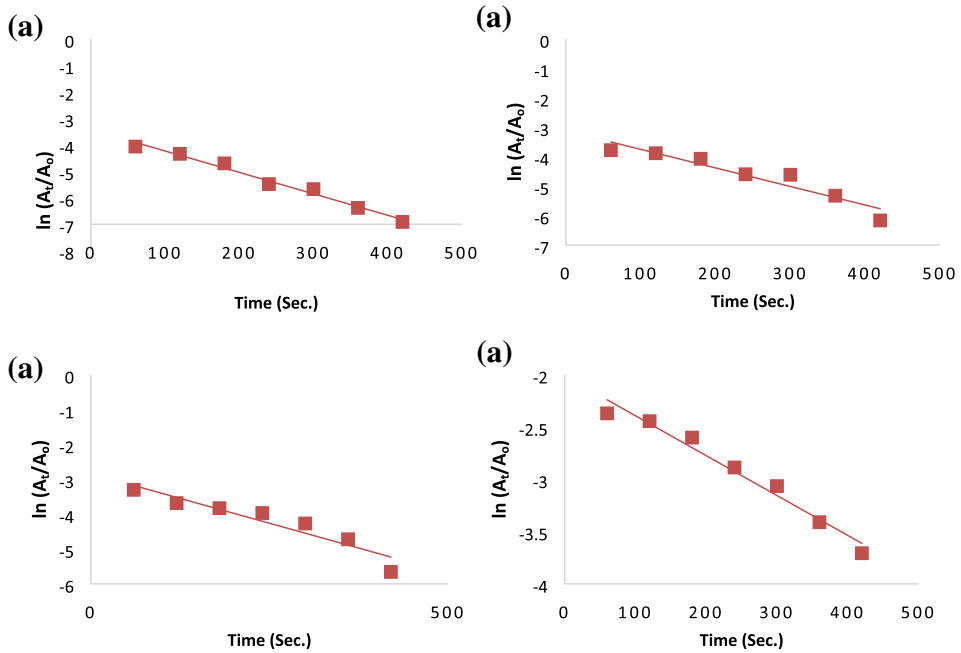


Fig. 12 Plot of ln At/Ao against time for different concentrations of 4-NP **a** 0.000125 **b** 0.00025 **c** 0.0005 **d** 0.001 mol/L using $[Cu_2(TDPH)_4(QNX)].DMF$ as catalyst

Table 3 Rate constants (k_{app}) and thermodynamic parameters for the reduction of 4-NP at different temperatures using $[Cu_2(TDPH)_4(QNX)].DMF$ as a catalyst

Parameters	$10^4 \times k_{app}$, s^{-1}
30 °C	8.0
40 °C	4.0
50 °C	3.0
60 °C	8.0

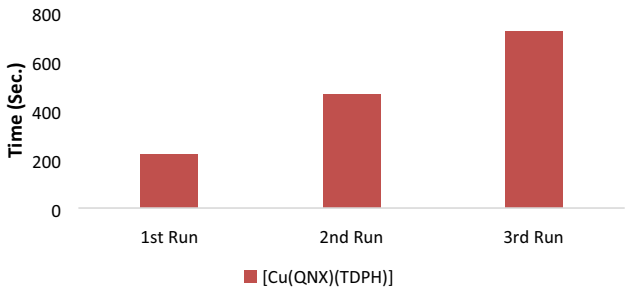


Fig. 13 Reusability experiments for the compound $[Cu_2(TDPH)_4(QNX)].DMF$

3.13 Comparison of the Activity of Various Catalysts for the Reduction of 4-Nitrophenol

The activity of the synthesized compound $[Cu_2(TDPH)_4(QNX)].DMF$ as a catalyst for the reduction of 4-nitrophenol to 4-aminophenol was compared with previously reported catalysts for the same reduction process using $NaBH_4$ as the reducing agent. As observed from Table 4, compound $[Cu_2(TDPH)_4(QNX)].DMF$ compared favourably well with the other catalysts. The rate constant obtained for the reduction process in the present study is higher (8.4×10^{-3} s^{-1}) when compared with the most recently reported catalysts [43, 44]. This result, therefore, indicates that compound $[Cu_2(TDPH)_4(QNX)].DMF$ is a better alternative to other effective catalysts reported for this reaction.

Table 4 Rate constants for the reduction reaction at different concentrations of 4-NP

4-NP conc. (mol L^{-1})	k (s^{-1})
0.000125	8.1×10^{-3}
0.00025	6.3×10^{-3}
0.0005	5.7×10^{-3}
0.001	3.8×10^{-3}

The ^1H NMR spectra of the 4-aminophenol product formed presents signal shifts: ^1H NMR (δ ppm in D2O) (δ, ppm) 1.8319 and 3.3575 ascribable to the amino- group chemical shifts [45]. These were observed to be absent in the ^1H NMR spectra of the 4-nitrophenol (Fig. S2) (Table 5).

4 Conclusions

This paper presents a new dinuclear Cu(II) coordination polymer, $[Cu_2(TDPH)_4(QNX)].DMF$**.** The structure of the compound was confirmed by single-crystal X-ray diffraction analysis. The two Cu(II) ions are present in the structure with each in the octahedral coordination. The compound was investigated as a catalyst for the conversion of 4-nitrophenol to the less toxic 4-aminophenol using $NaBH_4$ as the reducing

Content courtesy of Springer Nature, terms of use apply. Rights reserved.

Table 5 Comparison of the activity of various catalysts for catalysing the reduction of 4-NP

Catalysts	k_{app} (s^{-1})×10^{-3}	Refs.
$[Cu_2(TDPH)_4(QNX)_2]$.DMF	8.4	This work
RGO–$Ni_{25}Co_{75}$	1.55	Bai et al. [43]
Cu/Ag NPs	3.95	Wu et al. [44]

agent. The rate of the reduction process decreased with an increase in both temperature and 4-nitrophenol concentration. Compound $[Cu_2(TDPH)_4(QNX)]$.DMF was observed to be more efficient than most recently reported literature catalysts for the reduction reaction.

Supplementary Information The online version contains supplementary material available at https://doi.org/10.1007/s10904-021-01966-7.

Acknowledgements VOA is grateful to TWAS-CIIT for the 2017 TWAS-CIIT Fellowship award to carry out part of this research at the COMSATS Institute of Information Technology, Islamabad, Abbottabad Campus, Pakistan. Many thanks to Prof. M. Nawaz Tahir of the University of Sargodha, Pakistan, for helping out with the single-crystal X-ray diffraction analysis.

Declarations

Conflict of interest The authors state that there are no conflicts to declare.

References

1. A.C. Tella, S.O. Owalude, P.A. Ajibade, N. Simon, S.J. Olatunji, M.S.M. Abdelbaky, S. Garcia-Granda, J. Mol. Struct. **1125**, 570–575 (2016)
2. A.C. Tella, S.O. Owalude, S.J. Olatunji, V.O. Adimula, S.E. Elaigwu, L.O. Alimi, P.A. Ajibade, O.S. Oluwafemi, J. Environ. Sci. **6**, 264–275 (2018)
3. E.C. Constable, Chem. Soc. Rev. **42**, 1637–1651 (2013)
4. A.C. Tella, S.O. Owalude, C.A. Ojekanmi, O.S. Oluwafemi, New J. Chem. **38**, 4494–4500 (2014)
5. L. Ma, J.M. Falkowski, C. Abney, W. Lin, Nat. Chem. **2**, 838–846 (2010)
6. D. Chen, Y. Cao, N. Chen, P. Feng, J. Inorg. Organomet. Polym. (2021). https://doi.org/10.1007/s10904-020-01832-y
7. P. Horcajada, C. Serre, G. Maurin, N.A. Ramsahye, F. Balas, M. Vallet-Regi, M. Sebban, F. Taulelle, G. Férey, J. Am. Chem. Soc. **130**, 6774–6780 (2008)
8. C. Zhu, Q. Xia, X. Chen, Y. Liu, X. Du, Y. Cui, ACS Catal. **6**, 7590–7596 (2016)
9. H. Furukawa, K.E. Cordova, M. O'Keeffe, O.M. Yaghi, Science **341**, 974–975 (2013)
10. L. Zhang, S. Qiu, G. Jiang, G. Jiang, R. Tang, Asian J. Org. Chem. **7**, 165–170 (2018)
11. H.C. Zhou, J.R. Long, O.M. Yaghi, Chem. Rev. **112**, 673–674 (2012)
12. G. Maurin, C. Serre, A. Cooper, G. Férey, Chem. Soc. Rev. **46**, 3104–3107 (2017)
13. Y. Yang, X.X. Qi, H.R. Chen, X.Y. Wang, X.L. Yang, Y.Y. Tu, T. Zhou, T. Jiang, F. Wang, Z. Chen, Y.C. Ju, J. Inorg. Organomet. Polym. **30**, 4289–4296 (2020)
14. W. Lu, Z. Wei, Z.-Y. Gu, T.-F. Liu, J. Park, J. Park, J. Tian, M. Zhang, Q. Zhang, T. Gentle III., M. Boscha, H.-C. Zhou, Chem. Soc. Rev. **43**, 5561–5593 (2014)
15. J.X. Jiang, A. Trewin, D.J. Adams, A.I. Cooper, Chem. Sci. **2**, 1777–1781 (2011)
16. G. Cheng, T. Hasell, A. Trewin, D.J. Adams, A.I. Cooper, Angew. Chem. Int. Ed. **51**, 12727–12731 (2012)
17. M.D. Allendorf, C.A. Bauer, R.K. Bhakta, R.J.T. Houk, Chem. Soc. Rev. **38**, 1330–1352 (2009)
18. D. Maspoch, D. Ruiz-Molina, J. Veciana, Chem. Soc. Rev. **36**, 770–818 (2007)
19. C.L. Cahill, D.T. de Lilla, M. Frisch, CrystEngComm **9**, 15–26 (2007)
20. A.C. Tella, S.O. Owalude, M.F. Omotoso, S.J. Olatunji, A.S. Ogunlaja, L.O. Alimi, O.K. Popoola, S.A. Bourne, J. Mol. Struct. **1157**, 450–456 (2018)
21. X.B. Yin, Y.N. Song, Y. Wang, L.J. Zhang, Q.W. Li, Sci. China Chem. **57**, 135–140 (2014)
22. W.J. Zhang, D.Y. Li, B. Song, J. Inorg. Organomet. Polym. **30**, 3989–3998 (2020)
23. M.S. Deenadayalan, N. Sharma, P.K. Verma, C.M. Nagaraja, Inorg. Chem. **55**, 5320–5327 (2016)
24. A. Halder, S. Patra, B. Viswanath, N. Munichandraiah, N. Ravishankar, Nanoscale **3**, 725–730 (2011)
25. J. Jaramillo-García, V. Sanchez-Mendieta, I. García-Orozco, R.A. Morales-Luckie, D. Martínez-Otero, A. Téllez-López, L.D. Rosales-Vázquez, R. Escudero, F. Morales, Z. Anorg. Allg. Chem. **644**, 19–22 (2018)
26. N. Getachew, Y. Chebule, I. Diaz, M. Sanchez-Sanchez, J. Porous Mat. **21**, 769–773 (2014)
27. A. Nimmermark, L. Ohrstrom, J. Reedijk, Z. Kristallogr. **228**, 311–317 (2013)
28. S.E.H. Etaiw, M.M. El-bendary, J. Inorg. Organomet. Polym. **23**, 510–518 (2013)
29. A.C. Tella, A.C. Oladipo, V.O. Adimula, O.A. Ameen, S.A. Bourne, A.S. Ogunlaja, New J. Chem. **43**, 14343–14354 (2019)
30. A. Phan, A.U. Czaja, F. Gandara, C.B. Knobler, O.M. Yaghi, Inorg. Chem. **50**, 7388–7390 (2011)
31. X. Huang, S. Jiang, M. Liu, J. Phys. Chem. **109**, 114–119 (2005)
32. V.B. Nagaveni, K.M. Mahadevan, G.R. Vijayakumar, H. Nagabhushana, S. Naveen, N.K. Lokanath, JSAMD **3**, 51–58 (2018)
33. S.E.H. Etaiw, T.A. Fayed, D.M.A. El-Aziz, H.M. Khattab, J. Inorg. Organomet. Polym. (2021). https://doi.org/10.1007/s10904-020-01856-4
34. P. Horlescu, D. Sutiman, C.S. Stan, C. Mita, C. Peptu, M.E. Fortuna, C. Albu, Environ. Eng. Manag. J. **14**, 389–397 (2015)
35. F. Moura de Oliveira, L.R. Bezerra de Araújo Nascimento, C.M. Santos-Calado, M.R. Meneghetti, M.G. Angelo da Silva, Catalysts **6**(12), 215 (2016)
36. B. Angelov, A. Angelova, S.K. Filippov, T. Narayanan, M. Drechsler, P. Stepanek, P. Couvreur, S. Lesieur, J. Phys. Chem. Lett. **4**, 1959–1964 (2013)
37. A. Gangula, R. Podila, M. Ramakrishna, L. Karanam, C. Janardhana, A.M. Rao, Langmuir **27**, 15268–15274 (2011)
38. A.I. Ayad, D. Luart, A.O. Dris, E. Guénin, Nanomaterials **10**, 1169 (2020)
39. L. Yan, L. Liu, M. Yuan, R. Guo, Colloids Surf. A Physicochem. Eng. Asp. **417**, 18–25 (2013)
40. Y.S. Seo, E.-Y. Ahn, J. Park, T.Y. Kim, J.E. Hong, K. Kim, Y. Park, Y. Park, Nanoscale Res. Let. **12**, 7 (2017)

Content courtesy of Springer Nature, terms of use apply. Rights reserved.

41. R.K. Narayanan, S.J. Devaki, Ind. Eng. Chem. Res. **54**, 1197–1203 (2015)
42. N. Getachew, Y. Chebule, I. Diaz, M. Sanchez-Sanchez, J. Porous Mater. **21**, 769–773 (2014)
43. S. Bai, X. Shen, G. Zhu, M. Li, H. Xi, K. Chen, ACS Appl. Mater. Interfaces **4**, 2378–2381 (2012)
44. W. Wu, M. Lei, S. Yang, L. Zhou, L. Liu, X. Xiao, C. Jiang, V. Roy, J. Mater. Chem. A **3**, 3450–3455 (2015)
45. M. Tranchant, A. Serrà, C. Gunderson, E. Bertero, J. García-Amorós, E. Gómez, J. Michler, L. Philippe, Appl. Catal. A Gen. **602**, 117698 (2020)

Publisher's Note Springer Nature remains neutral with regard to jurisdictional claims in published maps and institutional affiliations.

Content courtesy of Springer Nature, terms of use apply. Rights reserved.

Terms and Conditions

Springer Nature journal content, brought to you courtesy of Springer Nature Customer Service Center GmbH (“Springer Nature”).
Springer Nature supports a reasonable amount of sharing of research papers by authors, subscribers and authorised users (“Users”), for small-scale personal, non-commercial use provided that all copyright, trade and service marks and other proprietary notices are maintained. By accessing, sharing, receiving or otherwise using the Springer Nature journal content you agree to these terms of use (“Terms”). For these purposes, Springer Nature considers academic use (by researchers and students) to be non-commercial.
These Terms are supplementary and will apply in addition to any applicable website terms and conditions, a relevant site licence or a personal subscription. These Terms will prevail over any conflict or ambiguity with regards to the relevant terms, a site licence or a personal subscription (to the extent of the conflict or ambiguity only). For Creative Commons-licensed articles, the terms of the Creative Commons license used will apply.
We collect and use personal data to provide access to the Springer Nature journal content. We may also use these personal data internally within ResearchGate and Springer Nature and as agreed share it, in an anonymised way, for purposes of tracking, analysis and reporting. We will not otherwise disclose your personal data outside the ResearchGate or the Springer Nature group of companies unless we have your permission as detailed in the Privacy Policy.
While Users may use the Springer Nature journal content for small scale, personal non-commercial use, it is important to note that Users may not:

1. use such content for the purpose of providing other users with access on a regular or large scale basis or as a means to circumvent access control;
2. use such content where to do so would be considered a criminal or statutory offence in any jurisdiction, or gives rise to civil liability, or is otherwise unlawful;
3. falsely or misleadingly imply or suggest endorsement, approval , sponsorship, or association unless explicitly agreed to by Springer Nature in writing;
4. use bots or other automated methods to access the content or redirect messages
5. override any security feature or exclusionary protocol; or
6. share the content in order to create substitute for Springer Nature products or services or a systematic database of Springer Nature journal content.

In line with the restriction against commercial use, Springer Nature does not permit the creation of a product or service that creates revenue, royalties, rent or income from our content or its inclusion as part of a paid for service or for other commercial gain. Springer Nature journal content cannot be used for inter-library loans and librarians may not upload Springer Nature journal content on a large scale into their, or any other, institutional repository.
These terms of use are reviewed regularly and may be amended at any time. Springer Nature is not obligated to publish any information or content on this website and may remove it or features or functionality at our sole discretion, at any time with or without notice. Springer Nature may revoke this licence to you at any time and remove access to any copies of the Springer Nature journal content which have been saved.
To the fullest extent permitted by law, Springer Nature makes no warranties, representations or guarantees to Users, either express or implied with respect to the Springer nature journal content and all parties disclaim and waive any implied warranties or warranties imposed by law, including merchantability or fitness for any particular purpose.
Please note that these rights do not automatically extend to content, data or other material published by Springer Nature that may be licensed from third parties.
If you would like to use or distribute our Springer Nature journal content to a wider audience or on a regular basis or in any other manner not expressly permitted by these Terms, please contact Springer Nature at

onlineservice@springernature.com